

Article

Synthesis of 3D Cadmium(II)-Carboxylate Framework Having Potential for Co-Catalyst Free CO₂ Fixation to Cyclic Carbonates

Zafar A. K. Khattak^{1,2}, Nazir Ahmad^{3,*}, Hussein A. Younus^{4,5}, Habib Ullah⁶, Baoyi Yu⁷,
Khurram S. Munawar⁸, Muhammad Ashfaq⁹, Sher Ali¹⁰, Hossain M. Shahadat¹¹ and Francis Verpoort^{1,12,*}

- ¹ State Key Laboratory of Advanced Technology for Materials Synthesis and Processing, Wuhan University of Technology, Wuhan 430070, China
² Institute of Chemistry, Baghdad-ul-Jadeed Campus, The Islamia University of Bahawalpur, Bahawalpur 63100, Pakistan
³ Chemistry Department, Government College University Lahore, Lahore 54000, Pakistan
⁴ Chemistry Department, Faculty of Science, Fayoum University, Fayoum 63514, Egypt
⁵ Department of Chemical and Petroleum Engineering, College of Engineering, Sultan Qaboos University, Al Khould, P.O Box 33, Muscat PC 123, Oman
⁶ Department of Material Science and Engineering, Chungnam National University, Daejeon 34134, Korea
⁷ Key Laboratory of Urban Agriculture (North China), Ministry of Agriculture, College of Biological Sciences Engineering, Beijing University of Agriculture, Beijing 102206, China
⁸ Department of Chemistry, University of Mianwali, Mianwali 42200, Pakistan
⁹ Department of Physics, University of Sargodha, Sargodha 40100, Pakistan
¹⁰ Department of Chemistry, Khushal Khan Khattak University Karak, Karak 27200, Pakistan
¹¹ Department of Chemistry, Faculty of Science, Comilla University, Comilla 3506, Bangladesh
¹² Research School of Chemical and Biomedical Technologies, National Research Tomsk Polytechnic University, Lenin Avenue 30, 634050 Tomsk, Russia
* Correspondence: dr.nazirahmad@gcu.edu.pk (N.A.); francis@whut.edu.cn (F.V.)



Citation: Khattak, Z.A.K.; Ahmad, N.; Younus, H.A.; Ullah, H.; Yu, B.; Munawar, K.S.; Ashfaq, M.; Ali, S.; Shahadat, H.M.; Verpoort, F. Synthesis of 3D Cadmium(II)-Carboxylate Framework Having Potential for Co-Catalyst Free CO₂ Fixation to Cyclic Carbonates. *Inorganics* **2022**, *10*, 162. <https://doi.org/10.3390/inorganics10100162>

Academic Editor: Navid Rabiee

Received: 31 August 2022

Accepted: 26 September 2022

Published: 1 October 2022

Publisher's Note: MDPI stays neutral with regard to jurisdictional claims in published maps and institutional affiliations.



Copyright: © 2022 by the authors. Licensee MDPI, Basel, Switzerland. This article is an open access article distributed under the terms and conditions of the Creative Commons Attribution (CC BY) license (<https://creativecommons.org/licenses/by/4.0/>).

Abstract: Metal-organic frameworks (MOFs) are porous coordination polymers with interesting structural frameworks, properties, and a wide range of applications. A novel 3D cadmium(II)-carboxylate framework, CdMOF ([Cd₂(L)(DMF)(H₂O)₂]_n), was synthesized by the solvothermal method using a tetracarboxylic bridging linker having amide functional moieties. The CdMOF crystal structure exists in the form of a 3D layer structure. Based on the single-crystal X-ray diffraction studies, the supramolecular assembly of CdMOF is explored by Hirshfeld surface analysis. The voids and cavities analysis is performed to check the strength of the crystal packing in CdMOF. The CdMOF followed a multistage thermal degradation pattern in which the solvent molecules escaped around 200 °C and the structural framework remained stable till 230 °C. The main structural framework collapsed (>60 wt.%) into organic volatiles between 400–550 °C. The SEM morphology analyses revealed uniform wedge-shaped rectangular blocks with dimensions of 25–100 μm. The catalytic activity of CdMOF for the solvent and cocatalyst-free cycloaddition of CO₂ into epichlorohydrin was successful with 100% selectivity. The current results revealed that this 3D CdMOF is more active than the previously reported CdMOFs and, more interestingly, without using a co-catalyst. The catalyst was easily recovered and reused, having the same performance.

Keywords: cadmium-organic framework; 3D framework; carbon dioxide fixation; cyclic carbonates synthesis; MOF catalysis

1. Introduction

In the last two decades, the porous MOFs and coordination polymers based on the self-assembly of metal ions or metal clusters and polydentate bridging ligands have attracted the incredible attention of material and supramolecular chemists worldwide, not only for their diverse and fascinating assemblies but also for their valuable properties required for various applications [1–5]. MOFs have emerged as an attractive class of materials that consists of an

infinite network synthesized from metal ions and multitopic organic linkers (ligands). In addition to relatively strong bonds between the inorganic (metal ions/clusters) and organic units (polydentate bridging ligands), the appropriate selection of these constituent units results in the reticular synthesis of MOFs of chemical and thermal stability with crystals of ultrahigh porosity. Solid materials other than MOFs do not usually offer the same accuracy normally required in chemical modifications. With the variation in chemical compositions and the shape of the building units based on specific structures, MOFs may result in compounds that have a synergistic mixture of features [6–9]. The variety of possibilities in the linking of these metal ions and organic linkers confers the MOFs with unique versatility in structure and density [10], adjustable surface properties [11], tunability in pore size [12], etc. This flexibility in structure and design makes MOFs an excellent material for potential applications in different areas, including energy storage devices, heterogeneous catalysis, gas adsorption/separation, chemical sensing, luminescence, magnetism, and biomedical applications, as MOFs are regarded as promising candidates for drug delivery and disease diagnosis [1,3,13,14]. Moreover, by controlling the functional groups and size of the organic linkers or changing metal nodes, MOFs can be tailored for any desired application [1,15–19]. The synthetic flexibility and unique structural diversity of MOFs make them more effective materials than microporous and mesoporous inorganic materials [20,21].

In the field of catalysis, MOFs have been investigated as heterogeneous catalysts or, in some cases, as catalyst supports for conventional organic transformations [1,8]. By taking advantage of using the metal of choice, the transition metal or main group metal, and the organic linkers, different MOFs have been successfully employed to catalyze different kinds of reactions to synthesize a large variety of compounds. Cd-based MOFs are mostly explored for their luminescence properties, which have potential applications in several fields, for example, chemical sensing, optoelectronics (ferroelectrics, LEDs, and non-linear optics), energy conversion and storage, biomedical applications, and so on [22,23]. However, Cd-based MOFs are less explored for catalysis. There are only a few reports on CO₂ fixation into epoxides to give cyclic carbonates [24–26]. In this work, novel CdMOF was synthesized by the solvothermal method and used as an active catalyst for the artificial fixation of CO₂ into cyclic carbonates. The catalyst showed good activity and selectivity without any co-catalyst or solvent. Moreover, the catalyst could be recycled without a noticeable decrease in activity or selectivity.

2. Experimental

4,4'-biphenyldicarbonyl chloride, 4-aminoisophthalic acid, triethylamine, methanol, *N,N'*-dimethylformamide (DMF), *N,N'*-dimethylacetamide (DMA), diethyl ether, and Cd(NO₃)₂·4H₂O were acquired from Aladdin. The chemicals were utilized without any additional purification.

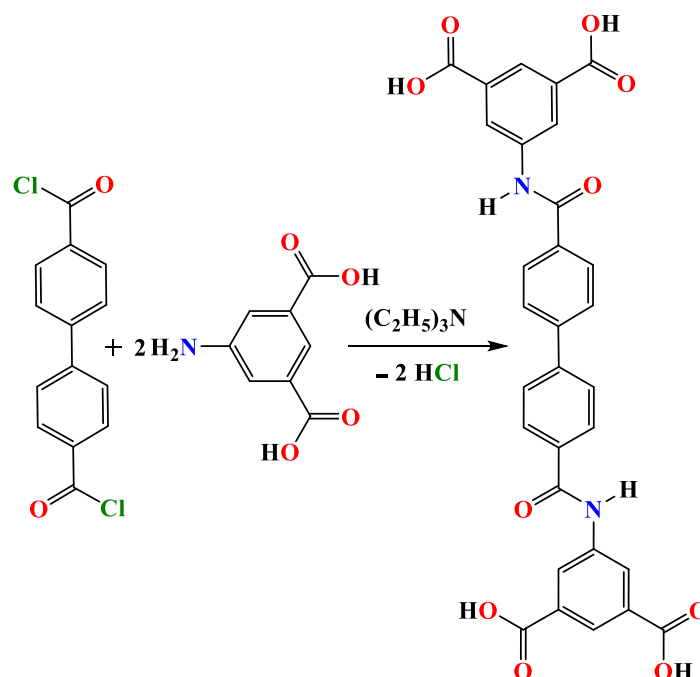
2.1. Characterization Methods

Fourier Transformer Infrared (FT–IR) spectra were recorded with the help of Thermo-Nicolet 6700 spectrometer over the 4000–400 cm^{−1} range. Inductively coupled plasma atomic emission spectroscopy (ICP–AES) was carried out employing an Optima 4300DV, Perkin Elmer wavelength coverage of 65–782 nm. The morphology of CdMOF was investigated employing Field Emission Scanning Electron Microscope (FE–SEM) images were taken on a ZEISS ULTRA PLUS-43-13 (OXFORD X-Max 50). Nuclear Magnetic Resonance spectra were acquired employing a 500 MHz Bruker Advance III-HD at room temperature. On a D8 Advance diffractometer (Bruker), a powder X-ray diffraction (XRD) investigation was carried out. Thermogravimetric analysis (TGA) of the samples was conducted utilizing a Netzsch STA 449C Jupiter Aeolos (German).

2.2. Synthesis of Ligand Acid (H₄L)

The ligand acid (H₄L) was synthesized by a reported procedure [27,28]. To a solution of 5-amino isophthalic acid (0.653 g, 3.6 mmol) and triethylamine (0.15 mL) in 20 mL of

DMA was added 4,4'-biphenyldicarbonyl chloride (0.506 g, 1.8 mmol), and stirred at room temperature for 16 hrs (Scheme 1). Then 50 mL of distilled water was added to the reaction mixture to settle down the product in the form of a white precipitate. After filtration, the white precipitates were washed with water, methanol, and ether and then dried in a vacuum. (Yield: 0.85 g, 83.5%). $^1\text{H-NMR}$ (DMSO- d_6 , δ ppm), Figure S1: 13.28 (s, 4H, -COOH), 10.69 (s, 2H, -CONH), 8.73 (d, 4H, ArH), 8.25 (t, 2H, ArH), 8.17 (d, 4H, ArH), 7.98 (d, 4H, ArH). $^{13}\text{C-NMR}$ (DMSO- d_6 , δ ppm), Figure S2: 167.0, 165.8, 142.7, 140.3, 134.2, 132.1, 130.5, 129.0, 127.5, 125.2. FT-IR (ν/cm^{-1}) Figure 1: 2983 (b), 1682 (s), 1607 (s), 1544 (vs), 1435 (s), 1320 (s), 1259 (s), 1130 (m), 1000 (m), 911 (m), 821 (vs), 751 (m), 661 (m), 597 (m). Elemental analysis for ligand, H_4L , $\text{C}_{30}\text{H}_{20}\text{N}_2\text{O}_{10}$ (%): Calculated: C, 63.38; H, 3.55; N, 4.93; and Found: C, 63.39; H, 3.56; N, 4.91 (For NMR spectra: see supporting information).



Scheme 1. Synthesis of ligand (H_4L).

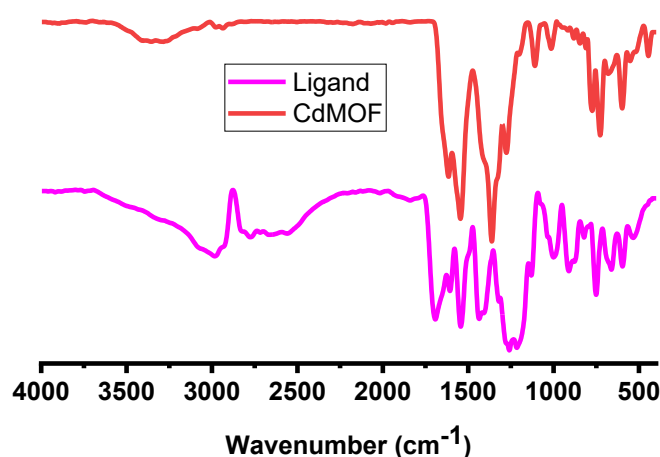


Figure 1. FT-IR spectra of ligand and as-synthesized CdMOF.

2.3. Synthesis of CdMOF ($[\text{Cd}_2(\text{L})(\text{DMF})(\text{H}_2\text{O})_2]_n$)

The ligand acid (H_4L) (0.075 mmol, 42.64 mg) was added to a mixture of DMF- H_2O (5 mL, 3:1 in v/v) in a 10 mL vial. To this solution, $\text{Cd}(\text{NO}_3)_2 \cdot 4\text{H}_2\text{O}$ (0.225 mmol, 69.41 mg) was added. One drop of concentrated HNO_3 was added to the reaction mixture and the

vial was then sealed. The reaction mixture was heated in an autoclave for two days at 70 °C, and colorless block crystals of CdMOF were obtained. The crystals were washed with DMF, followed by methanol, and then dried in the air. (Yield: 41 mg, 61 % based on H₄L). FT-IR (ν/cm^{-1}) Figure 1: 1652 (s), 1561 (s), 1509, 1436, 1384, 1265, 1104, 943, 895, 828, 747, 716, 684, 649 and 415 cm^{-1} . Elemental analysis for CdMOF, C₃₃H₂₇Cd₂N₃O₁₃ (%): Calculated: C, 44.12; H, 3.03; N, 4.68; and Found: C, 42.39; H, 4.178; N, 6.17 (See note of the Table S1).

2.4. Catalytic Reactions

For the catalytic carboxylation reaction, 18 mmol of the substrate and 100 mg of MOFs were taken in a 30 mL stainless steel reactor (from XINGDA, Beijing, China), and heated at 120 °C under 8 bar pressure of CO₂. After finishing the reaction time, the reactor was allowed to come to room temperature. The surplus CO₂ was released from the reactor and the catalyst was recovered from the reaction mixture by centrifugation. The product obtained was characterized by ¹H-NMR using deuterated chloroform. For recycling, the catalyst recovered through centrifugation was thoroughly washed thrice with methanol followed by drying in vacuum oven at 80 °C for four hours.

3. Result and Discussion

3.1. Characterizations of CdMOF

Organic bridging ligands containing multiple carboxylic acid moieties have been extensively exploited for the synthesis of numerous MOFs [1,29]. Here we have synthesized a tetracarboxylic acid ligand (H₄L) containing amides functionalization connected through a long chain of phenyl rings (Scheme 1) [27,28]. [Cd₂(L)(DMF)(H₂O)₂]_n (CdMOF) was synthesized using the reported procedure [30] via the reaction of cadmium nitrate with ligand, H₄L. The synthesized MOF was characterized by single-crystal XRD, powder XRD, FT-IR, XPS, SEM, and TGA.

FT-IR spectrum shows a significant shift of carbonyl group vibrating frequency (ν/cm^{-1}) towards lower wavenumber from 1689 to 1652 cm^{-1} in the CdMOF as compared to that of acid ligand (Figure 1). Furthermore, the peak visible around 415 cm^{-1} is assigned to Cd-O which suggests the formation of CdMOF. The colorless block crystals obtained through the solvothermal method were analyzed by single crystal x-ray diffraction. The observed powder XRD data of the as-synthesized sample was compared with the simulated PXRD (as obtained from the single crystal XRD) of CdMOF as presented in Figure 2. The complete match of the peaks in both cases shows the bulk phase purity of the as-synthesized CdMOF sample.

The single crystal X-ray diffraction analysis shows that the structure of CdMOF is a 3D framework in the monoclinic crystal system with space group $P2_1/n$ (Table S1). The asymmetric unit consists of one ligand (C1-C30/N1/N2/O1-O10), one anionic *N,N'*-dimethyl formamide (DMF) solvent (N3A/C31-C33/O00C), two metal centers (Cd1/Cd2) and two water molecules (O11/O12) that are coordinated to cadmium (Cd1) (Figure 3). The O-atoms of amide groups are not involved in coordination with the Cd-cations. The first metal atom (Cd1) is coordinated by O-atoms of two water molecules, the O-atom of a DMF as a coordinating solvent, and three O-atoms of the carboxylate group of three individual ligands (L⁴⁻). Thus (Cd1) is hexa coordinated to form an octahedral geometry as shown in Figure 3b. The second metal atom (Cd2) is coordinated by carboxylate O-atoms of five independent ligands (L⁴⁻), whereas the O-atom of DMF is not involved in the coordination with Cd-atom (Cd2). Two out of five ligands (L⁴⁻) are coordinated with the (Cd2) atom in a chelating fashion. So, the (Cd2) atom is hepta coordinated to form a distorted pentagonal bipyramidal geometry. In the CdMOF 3D framework structure (Figure 4), the Cd-O bond lengths and bond angles of the coordination sphere in CdMOF (Table S2) are in agreement with the corresponding bond lengths and bond angles in similar CdMOF crystal structures [31–34]. The carboxylate groups A (C7/O1/O2) and B (C8/O3/O4) are oriented at the dihedral angle of 7.3 (2)° and 21.1 (2)° with respect to the parent phenyl ring C (C1–C6). The benzamide group D (C9-C15/N1/O5) makes

the dihedral angle of $42.4(5)^\circ$ with the root mean square plane of the second benzamide group E (C16/C22/N2/O6). The O-atom of group D maximum deviates from the root mean plane of group D with a deviation of $0.4360(8) \text{ \AA}$ whereas the N-atom of group E maximum deviates from the root mean plane of group E with a deviation of $0.259(9) \text{ \AA}$. The carboxylate groups F (C30/O7/O8) and G (C29/O9/O10) are oriented at the dihedral angle of $8.9(2)^\circ$ and $2.9(2)^\circ$ with respect to the parent phenyl ring H (C23-C28) which indicate that group F and G are almost planar to ring H. The carbonyl group (C22/O6) of group E and the dimethylamine (N3A/C32/C33) of coordinating a DMF solvent are disordered with an occupancy ratio of $0.66(3):0.34(3)$ and $0.68(2):0.32(2)$, respectively.

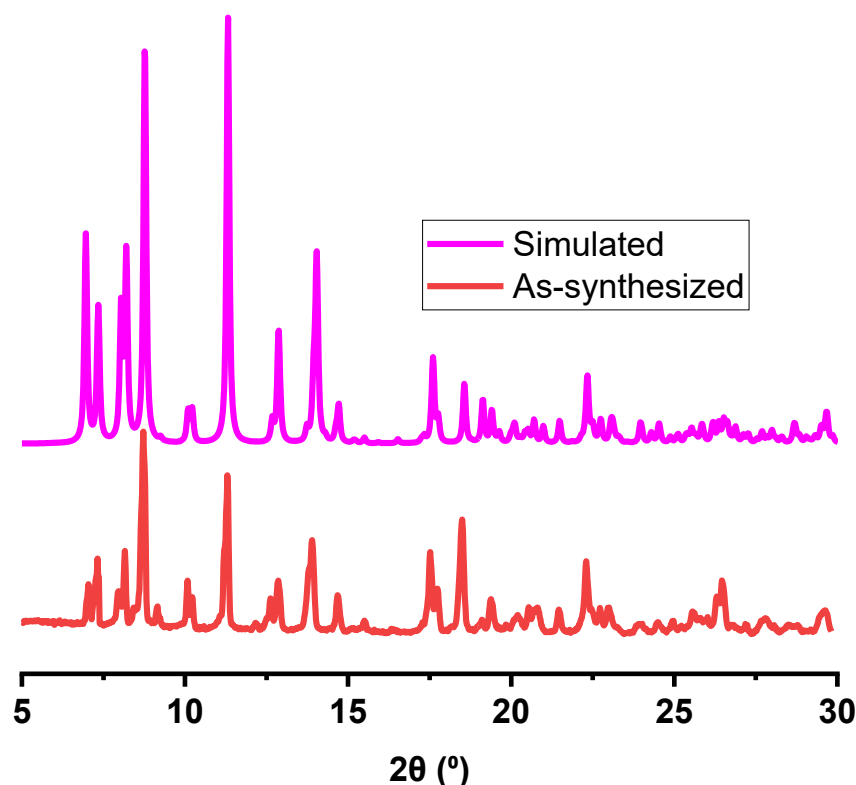


Figure 2. Powder XRD spectra of the as-synthesized and simulated CdMOF.

From the literature point of view, four (04) MOF crystal structures are found that have close similarities with the crystal structure of CdMOF. These MOFs' crystal structures have the same and/or similar fully deprotonated organic linker (H_4L , amide containing tetracarboxylic ligand) as in CdMOF but have different metal centers. Mn(II)-MOF, $[Mn_2(L)(H_2O)_3] \cdot (H_2O)_{4.8}$ is a 3D framework having a triclinic crystal system with space group $P\bar{1}$ and $Z = 2$ [35], Co(II)-MOF $\{[Co_2(L)(H_2O)_3] \cdot S_x\}_n$ is a 3D framework structure of monoclinic crystal system having $P2_1$ and $Z = 1$, [28], and both the Cd(II)-MOF [30] and the Zn(II)-MOF, $Cd(L) \cdot (HDMA)_2(DMF)(H_2O)_3$ and $Zn(L) \cdot (HDMA)_2(DMF)(H_2O)_6$, respectively, are 3D frameworks with triclinic crystal systems with $P\bar{1}$ space groups and $Z = 2$ [30]. In all these selected crystal structures, the coordination geometry around metal centers is octahedral and the crystal structure exhibits a 3D framework. However, only in the crystal structure of Mn(II)-MOF, one of the O-atom of amide groups is involved in coordination with the metal center. The intermolecular H-bonding of type $O-H \cdots O$ and comparatively weak $C-H \cdots N$ and $C-H \cdots O$ are responsible for the crystal packing as given in Table S3 and shown in Figure S3. The crystal structure of CdMOF possesses a large channel along a -axis (Figure 5). The pore size calculated by using X-rays diffraction data is $13.2 \times 7.16 \text{ \AA}^2$. Inside the channel, there are the coordinated and the guest solvent molecules (DMF and H_2O) that help in stabilizing the 3D framework.

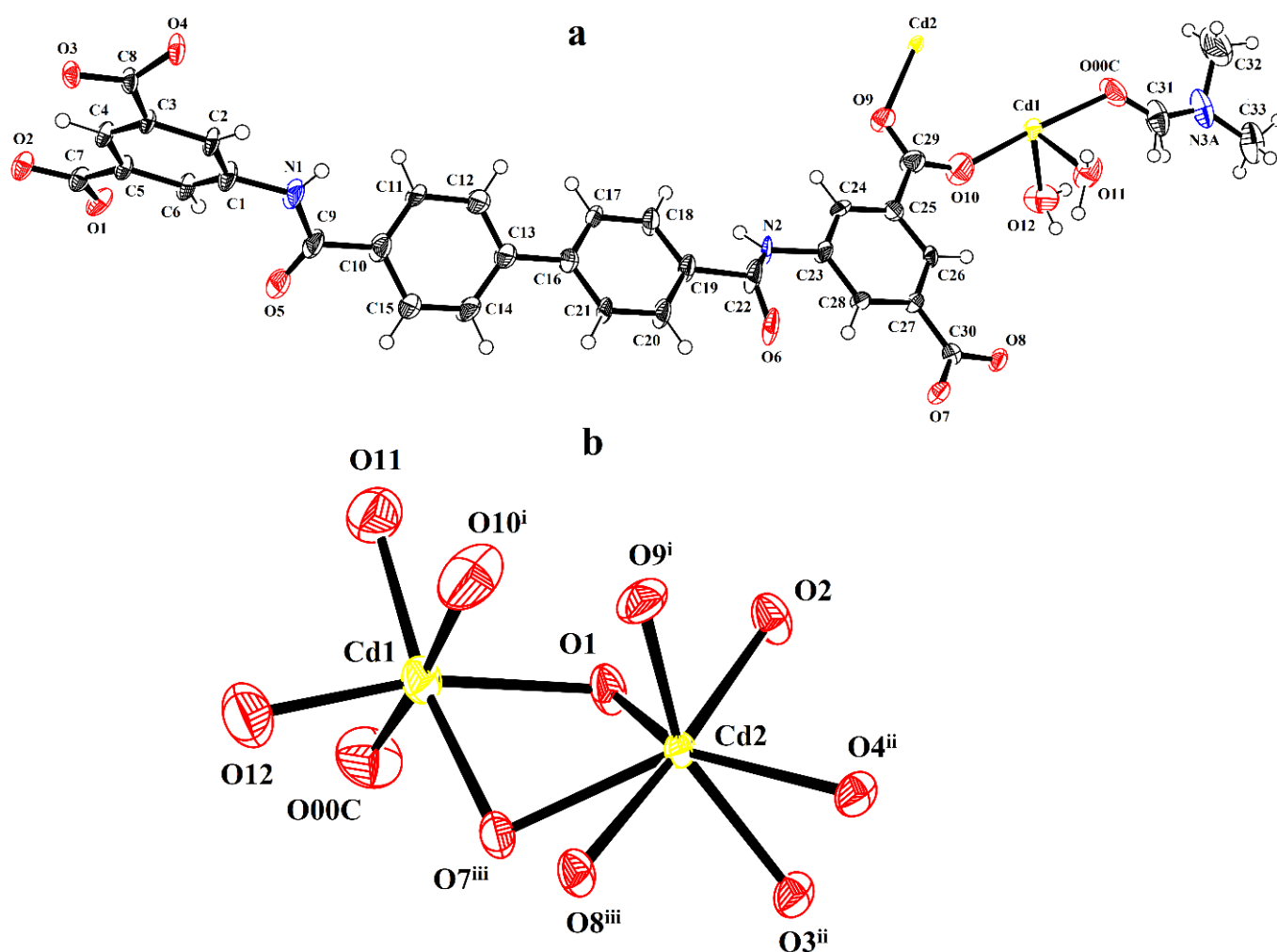


Figure 3. (a) ORTEP diagram of the asymmetric unit of CdMOF drawn at a probability level of 50%. H-atoms are shown by small circles of arbitrary radii, (b) Graphical representation of coordination sphere of Cd-1 and Cd-2 atoms in CdMOF, symmetry codes are (i) $x, y, -1 + z$, (ii) $1/2 - x, -1/2 + y, -1/2 - z$, (iii) $3/2 - x, -1/2 + y, \frac{1}{2} - z$.

The major factor that controls the properties of the MOF single crystals is the non-covalent interactions. In this perspective, we are exploring the non-covalent interactions in CdMOF by using comparably a new sort of analysis known as Hirshfeld Surface Analysis. The calculations are done by using Crystal Explorer software with version 21.5 [36–38]. Plotting a Hirshfeld surface (HS) by using the property of (normalized distances) d_{norm} exhibits interatomic contacts by colors. Ultimately, the information on the interatomic contacts is helpful in the understanding of the H-bonding interactions. The interatomic interactions for which the distance between interacting atoms is less than, equal to, or larger than the total of the atoms' van der Waal radii are depicted on the HS in the colors red, white, and blue, respectively. Figure 6a represents HS plotted over d_{norm} for CdMOF.

A deep red spot around Cd-atoms indicates that these atoms will be linked with the symmetry-related O-atoms. Similarly, the red spot around N-atom (N3), O-atom (O00C), carbonyl O-atoms (O3/O6/O7) and H-atoms of coordinating water (H12A/H12B) inferred their involvement in the in H-bonding (Figure 6a). By using HS plotted over shape index, weak interactions between molecules, such as $\pi \cdots \pi$ stacking interactions, may also be shown. Around the aromatic rings, there are contiguous triangular-shaped red and blue patches, which suggests the presence of $\pi \cdots \pi$ in the crystal packing. Such areas

surrounding the phenyl rings demonstrate the presence of the $\pi \cdots \pi$ stacking interaction in the compound's crystal packing (Figure 6b).

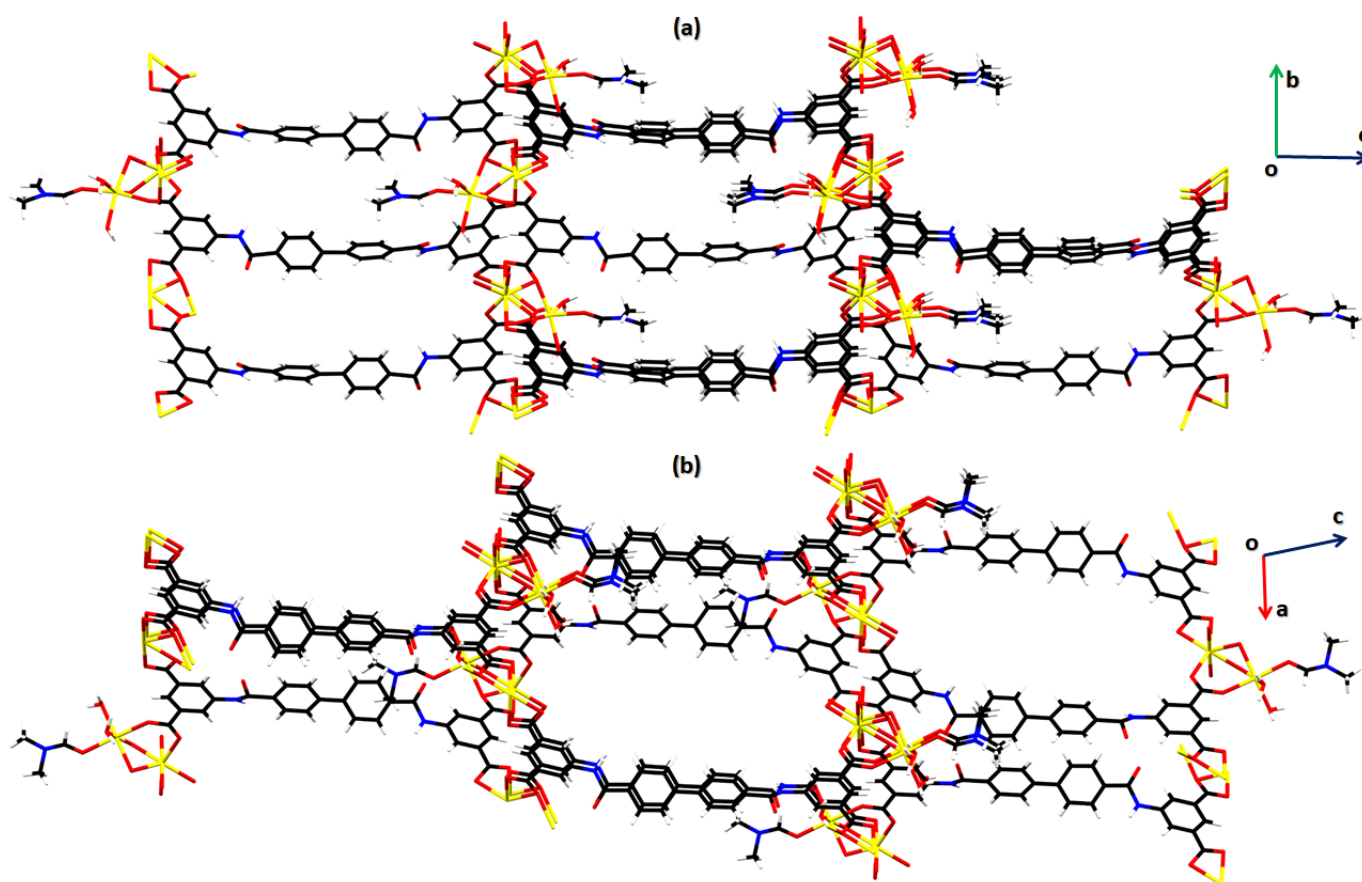


Figure 4. Graphical representations of the CdMOF 3D framework structure viewed along (a) *a*-axis, (b) *b*-axis.

The decomposition of the overall interatomic contacts to the separate interatomic contacts can be done by 2D fingerprint plots analysis which helps in the understanding of the supramolecular assembly in single crystals [39–45]. The 2D plot of the total interactions for CdMOF is displayed in Figure 7a. The existence of the center triangular area, which is colored sky-blue, shows that crystal packing exhibit $\pi \cdots \pi$ stacking interaction. $H \cdots H$ contacts contribute the most to the crystal packing of the compound, with a percentage contribution of 23.2% (Figure 7b) for CdMOF, it is the most crucial and significant interatomic contact. In addition to the $H \cdots H$ contacts, the $O \cdots H$ and $C \cdots H$ contacts are also crucial in defining the crystal packing with percentage contributions of 22.2% and 13.3%, respectively (Figure 7c,d). The 2D plots of the other interatomic contacts and their contribution to defining the crystal packing are shown in Figure 7d,e,i.

Supramolecular response of the CdMOF can be further explored by investigating atom-ALL and All-atom types of interactions. The interaction of the HS containing an atom with all the molecules present in the vicinity of HS is represented by atom-ALL interaction. Likewise, the interaction of all the atoms in HS to an atom present in the vicinity of HS is represented by ALL-atom interaction [46,47]. For both types of interactions, the interaction that involves H-atoms is strongest. The contribution of H-ALL and ALL-H interactions is 50.1% and 53.7%, respectively as shown in Figure 8. The contribution of all other interactions in defining the crystal packing is shown in Figure 8.

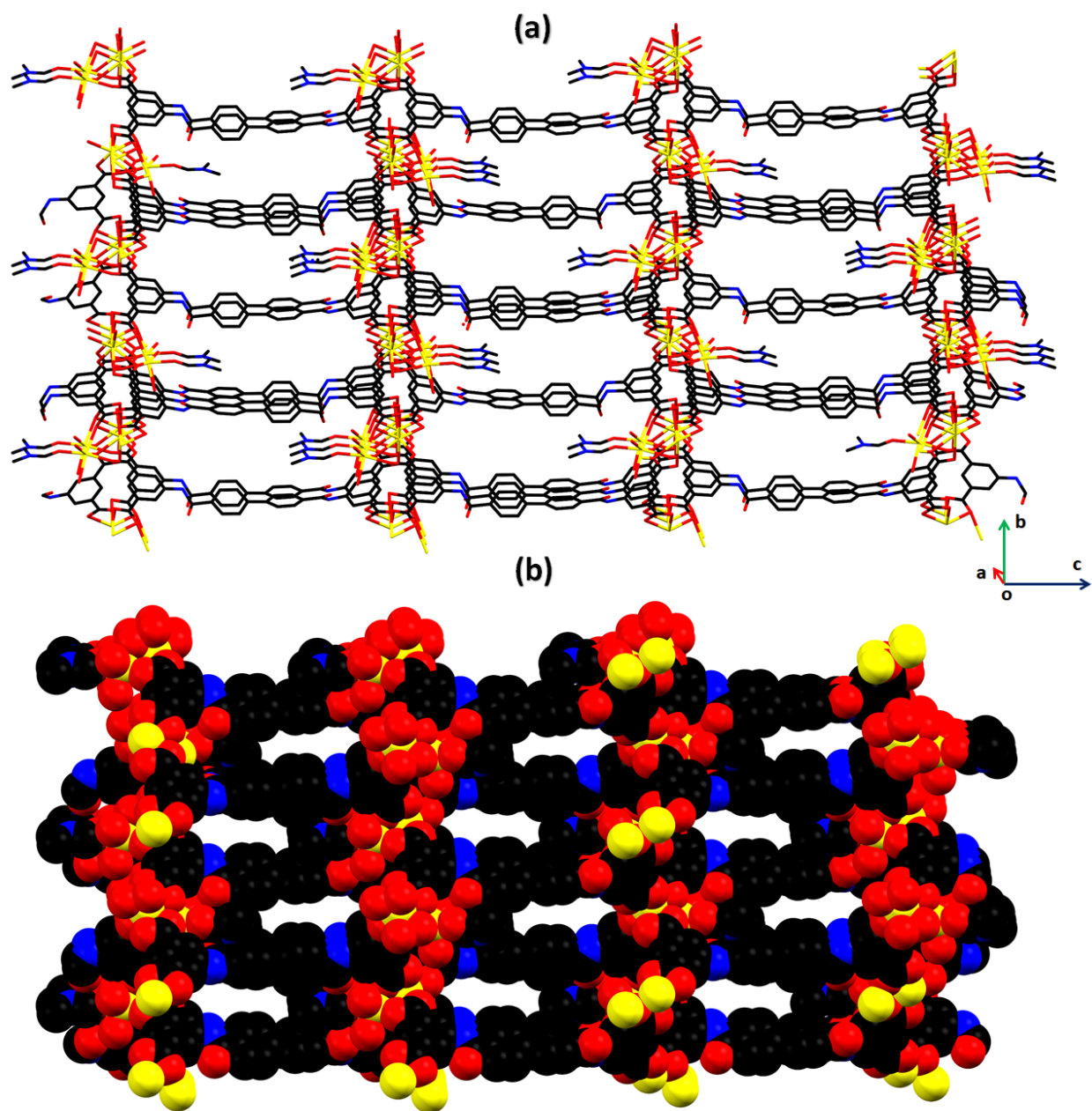


Figure 5. (a) X-rays crystal structure of CdMOF showing channels along the a-axis. (b) CPK model showing the dimensions of the channel windows (13.164×7.157) \AA^2 along the a-axis. H-atoms and minor parts of disordered atoms are not shown for clarity.

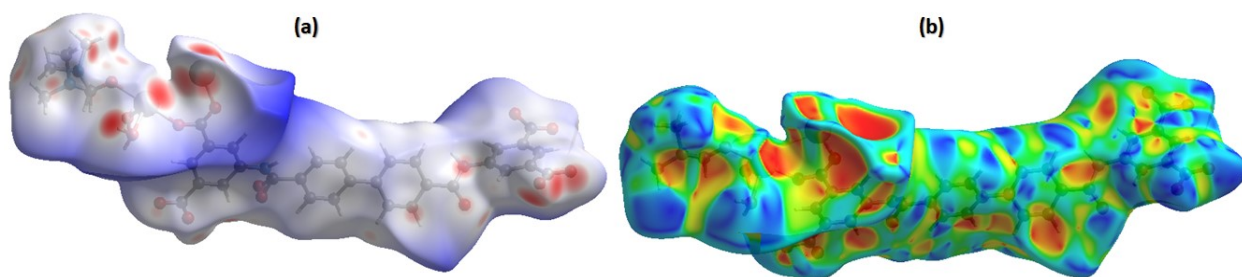


Figure 6. Hirshfeld surface plotted over d_{norm} (a) for CdMOF in the range -0.524 to 3.787 a.u. (b) Hirshfeld surface plotted over shape index in the range -1 to 1 a.u.

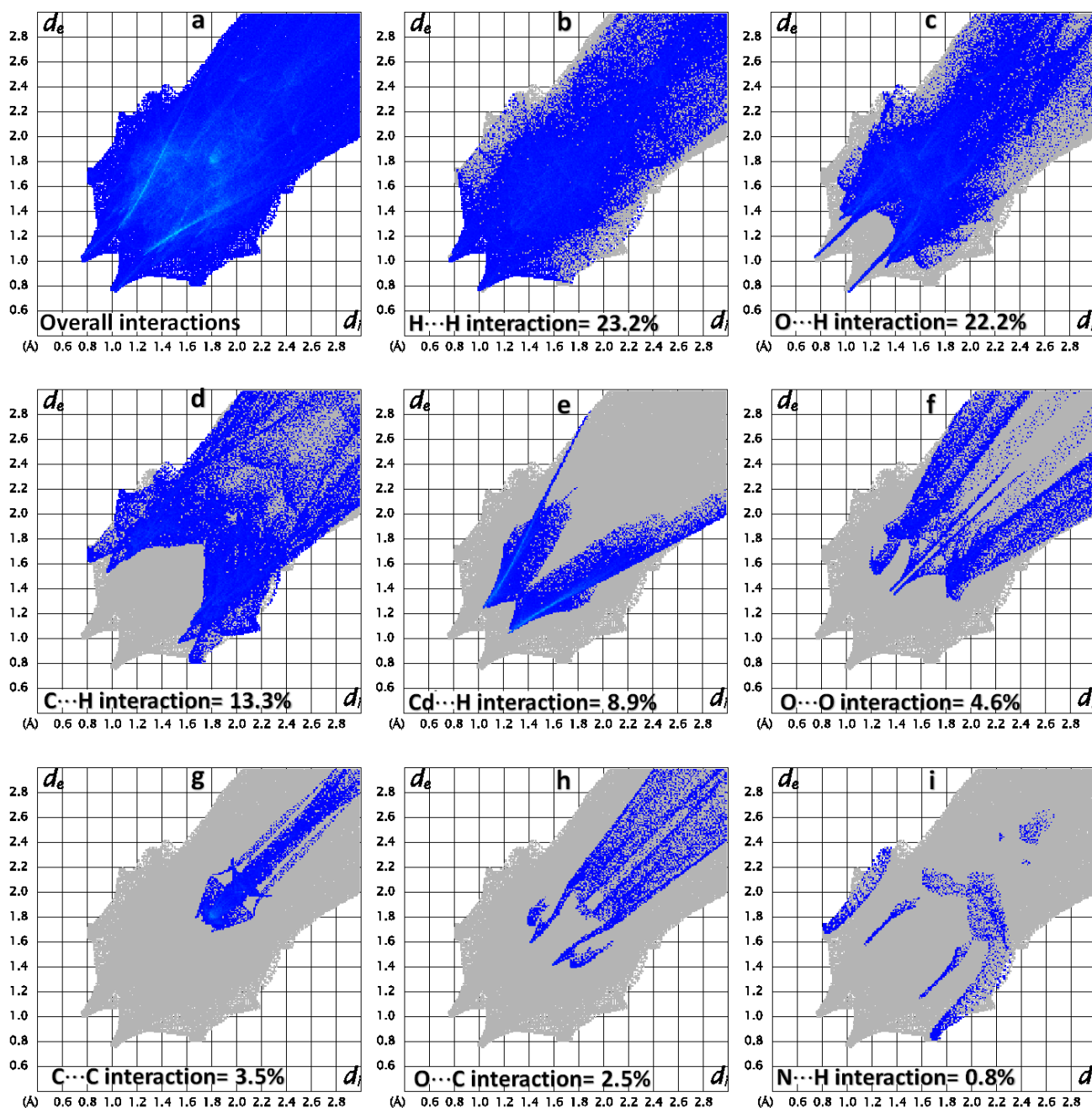


Figure 7. 2D fingerprint plots of CdMOF, for (a) Overall interactions, and (b–i) individual interatomic contacts with percentage contribution in the crystal packing greater than 0.7%.

The voids are crucial to investigate as far as the crystal packing of the single crystals is concerned because these empty spaces in single crystals provide a direct hint of the properties of the single crystals. We calculate voids in CdMOF (Figure 9a) by assuming that all the atoms are spherically symmetric and by using the Hartree–Fock theory [48,49]. The void volume is found to be 1520.52 \AA^3 and the unit cell volume is 4431.7 \AA^3 . The voids occupy $(1520.52/4431.7 \times 100\% = 34.3\%)$ of space in the crystal packing. The space occupied by voids in the crystal packing of CdMOF is large because the MOF has a porous structure and contained cavities which are obvious in Figure 9a. In order to further investigate the cavities, crystalmaker version 10.7.3 is used. The center of the cavity is represented by dummy atom Zz (Figure 9b). The size of cavities ranges from 2.8 \AA^3 to 4 \AA^3 .

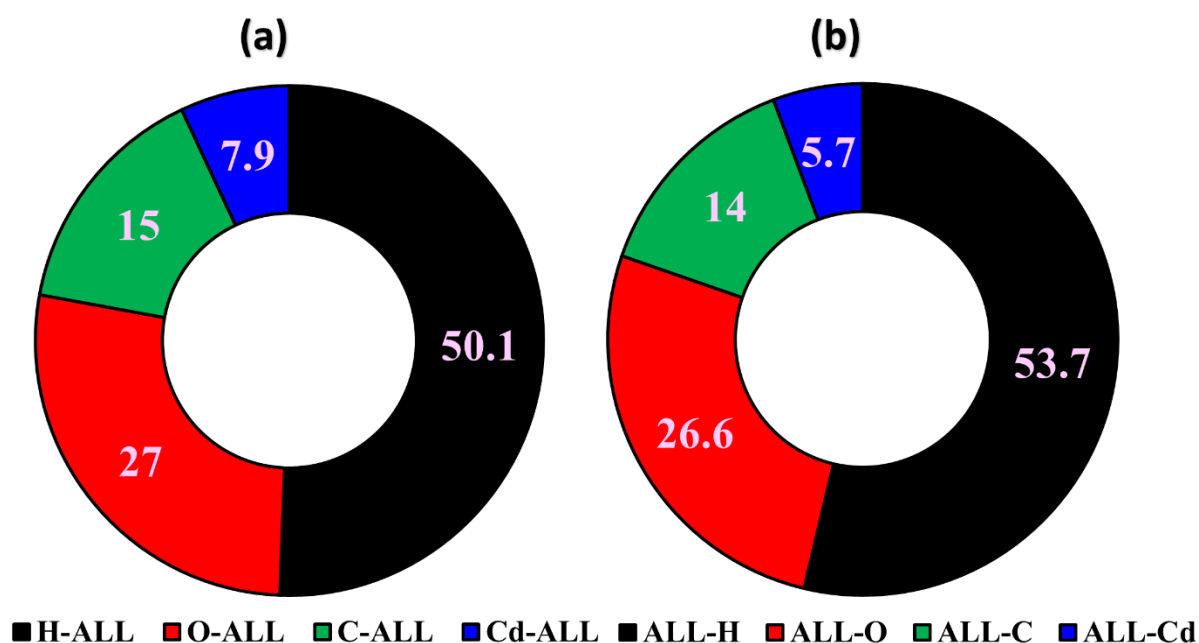


Figure 8. (a) Percentage contributions of the interaction of an atom present inside the HS to all the atoms present in the surroundings of the HS for CdMOF. (b) Percentage contributions of the interaction of all the atoms present inside the HS to an atom outside the HS for CdMOF.

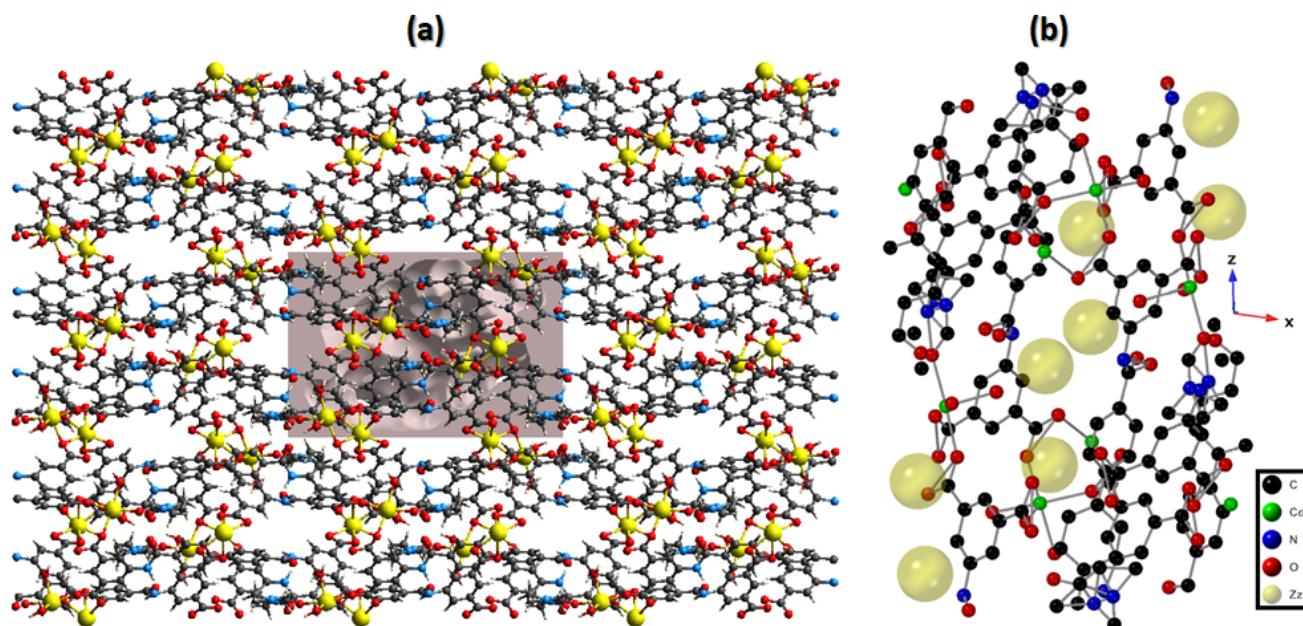


Figure 9. (a) Graphical representation of voids analysis along *bc* crystallographic plane for CdMOF (b) cavities shown as dummy atoms *Zz*.

The scanning electron microscopic (SEM) analysis was performed, and the characteristics of shape and surface morphology were revealed, which show uniform wedge-shaped rectangular blocks with dimensions of 25–100 μm . As shown in Figure 10. The XPS survey revealed that the sample has Cd, C, N, and O atoms (Figure 11a). The high-resolution XPS of the Cd3d region has peaks at 404.58 (Cd3d_{5/2}) and 411.18 (Cd3d_{3/2}) eV, well separated spin-orbit components ($\Delta = 6.6$ eV). Peaks are of symmetric shape, loss features are absent on the higher binding energy side of the 3d_{3/2} spin-orbit component for coordinatively bound Cd(II) Figure 11b. C1s spectrum (Figure 11c) typically consists of C-C

and O-C=O components. The peak at the binding energy of 283.38 eV corresponds to the C-C component by default, and the O-C=O component at 286.98 eV is observed [25]. C1s spectra reveal the polymeric nature as these are symmetric peak components. The extended delocalized electrons in the sample (i.e., aromatic rings) are expressed in the satellite feature, several eV away from the higher binding energy of the main peak. The π - π^* satellite is seen around 7.6 eV from the main C1s peak in CdMOF, as seen at 6 eV from C1s of polyethylene terephthalate, for example [50]. O1s peaks tend to be broad (Figure 11d), with multiple overlapping components. Components due to the ligands, DMF, and water overlap directly with each other. The oxygen (O1s) in the bound form to metal is observed as a broad peak at 530.48 eV. The peak becomes much broader due to H-O-C bonding. The N1s XPS peaks (Figure 11e) at 399.9 and 404.48 eV in CdMOF arise from the ligand and coordinated DMF, which is present in amide form. The N1s region may be overlapped by peaks from cadmium (404.48 eV) encompassing the weak π - π^* satellite features like nitrogen-containing aromatic polymers (e.g., polyimide).

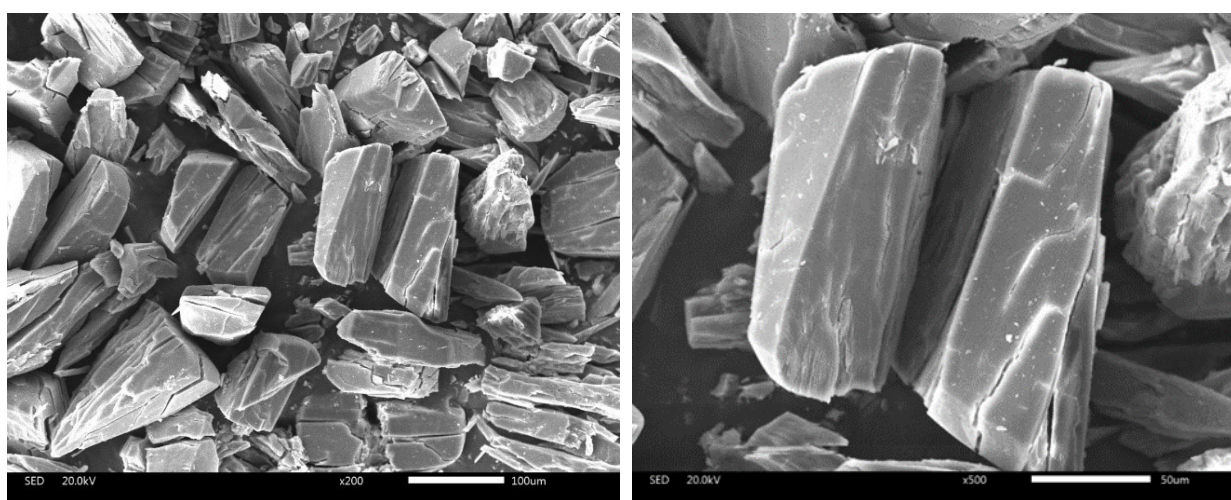


Figure 10. SEM Analysis of CdMOF at different resolutions.

The thermal stability of CdMOF was studied by thermogravimetric analysis. CdMOF followed a multistage thermal degradation pattern, as shown in Figure 12. At around 200 °C, the initial weight loss (<10%) is associated with the loss of solvent molecules. The structural framework remained stable till 230 °C. The two decomposition steps, between 400–550 °C, result in the collapses (>60 wt.%) of the main structure to organic volatiles. Hence, the structure of CdMOF remains intact till 200 °C, and the thermally stimulated fragmentation of the bridging organic linkers took place above this temperature, resulting in the breakdown of the main MOF structure. The TGA and DTG are shown in Figure 12. The remaining material (12.8%) is expected to be a metal oxide.

3.2. Catalytic Activity of CdMOF

The catalytic activity of CdMOF for the solvent and cocatalyst-free cycloaddition of CO₂ into epichlorohydrin was successful with 100% selectivity. The catalyst was easily recovered and reused, having the same performance. The catalytic cycloaddition of CO₂ was investigated in detail using epichlorohydrin as a substrate. Table 1 shows the conversion and selectivity of cyclic carbonate under the given conditions. There was no significant yield for the product in the presence of Cd(NO₃)₂·4H₂O as a catalyst. The cycloaddition of epichlorohydrin (18 mmol) in the presence of CdMOF (100 mg) gives better results at 120 °C and a CO₂ pressure of 8 bars (entry 1, Table 1). Even the recycled CdMOF under the given conditions gives reproducible results (entry 2, Table 1).

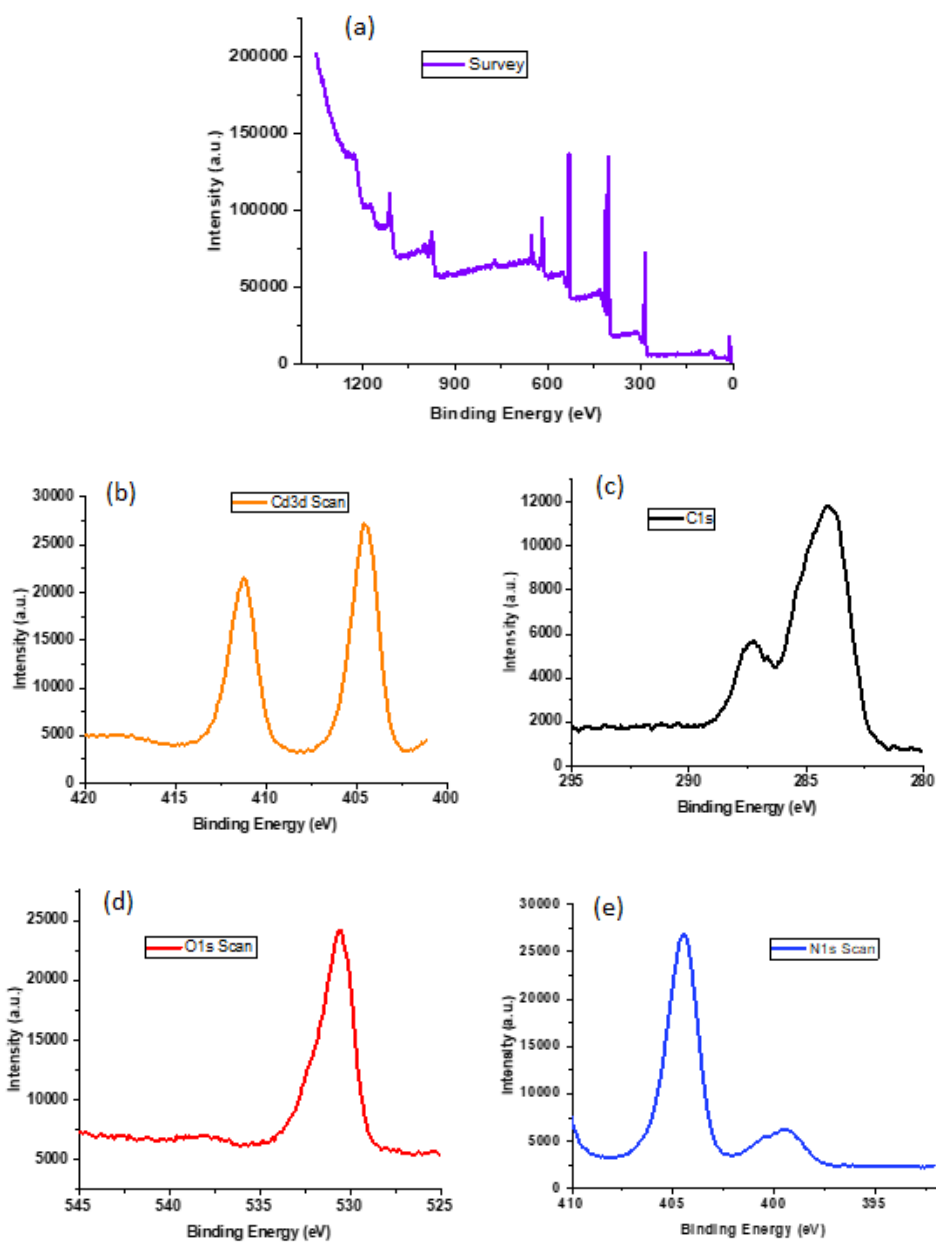


Figure 11. XPS analysis of CdMOF (a) Survey, (b) Cd 3d (c) C 1s, (d) O 1s, and (e) N 1s region.

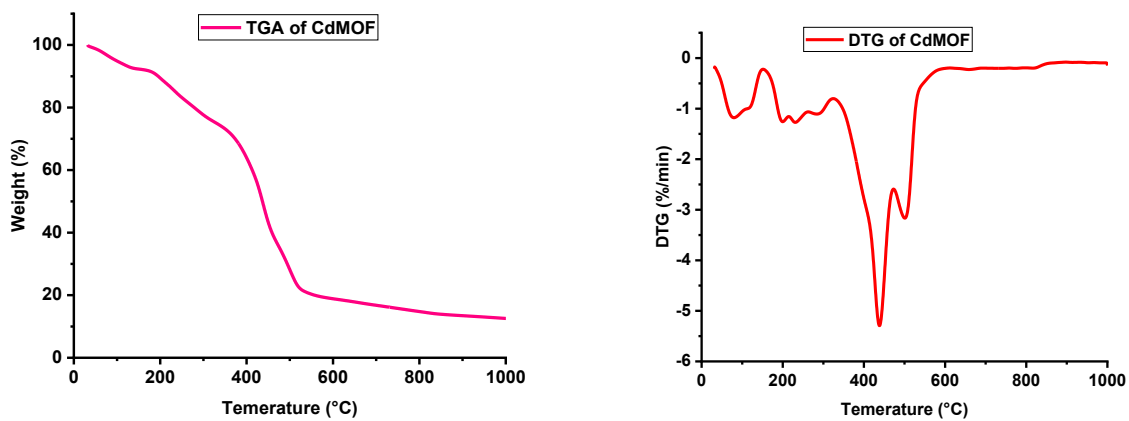


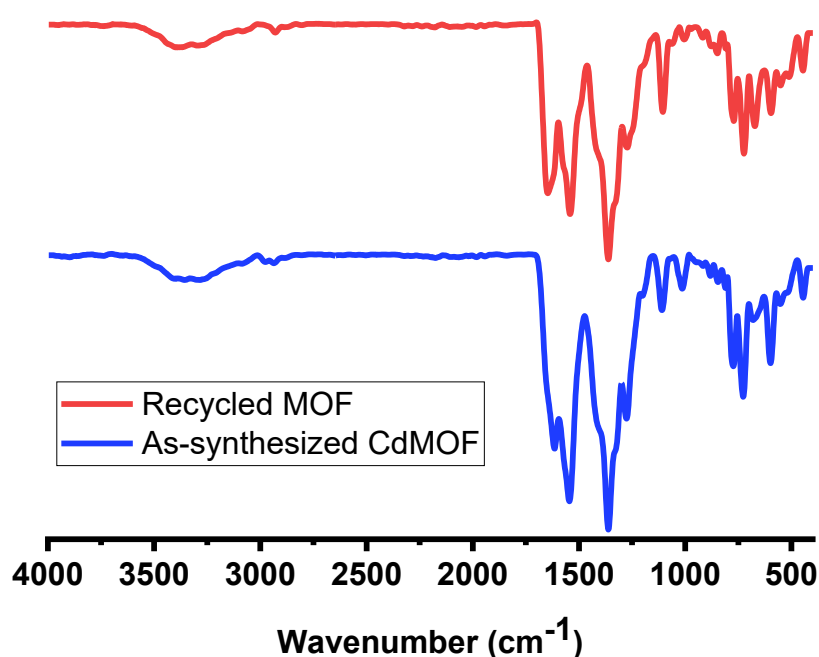
Figure 12. TGA and DTG analysis of CdMOF.

Table 1. Cycloaddition of CO₂ to epichlorohydrin catalyzed by CdMOF without cocatalyst and its a comparison with other CdMOFs.

Catalyst/Co-Catalyst	Catalyst Loading (mol%)	T (°C)	P (bar)	t (h)	Conversion (%)	Selectivity (%)	Reference
Control (without catalyst)	-	120	8	12	0	0	This work
3D CdMOF	0.67	120	8	12	83	100	This work
3D CdMOF ^a	0.67	120	8	12	82	100	This work
Cd(NO ₃) ₂ ·4H ₂ O	0.60	80	4	8	21	98	[25]
3D PNU-22 (a CdMOF) ^b	0.60	80	4	8	32	>99	[25]
3D PNU-22/TBAB ^c	0.60 ^f	80	4	8	85	>99	[25]
2D {[Cd(CHDC)(L)]·H ₂ O} _n ^d / TBAB	1.8 ^f	80	10	18	89	-	[24]
3D [Cd ₂ (Ni(salen))(DMF) ₃]·4DMF·7H ₂ O ^e / TBAB	0.50 ^f	80	10	12	99	-	[26]

^a Catalyst/CdMOF was recovered and reused, ^b [Cd₂(Hstdb)(stdb)(8H-Ade)(Ade)]_n, ^c *tetra*-Butylammonium bromide, ^d H₂CHDC = 1,4-cyclohexanedicarboxylic acid and L = *pyridyl*carboxaldehyde isonicotinoylhydrazone, ^e H₆salen = (R,R)-*N,N'*-bis(3-*tert*-butyl-5-(3,5-dicarboxybenzyl)salicylidene)-1,2-diphenylethylenediamine], ^f same for both catalyst and co-catalyst.

To minimize the environmental issues and energy requirements, the isolation of heterogeneous catalysts and, subsequently, their reusability is an important protocol in the lab and industrial processes. Recycling and reusability of CdMOF were carried out using epichlorohydrin as a substrate. After the completion of the catalytic reaction, the catalyst was recovered through centrifugation, thoroughly washed with methanol, and then dried under a vacuum for four hours before starting the new cycle. The recovered CdMOF after 3 catalytic cycles was characterized using FT-IR and PXRD (See Figures 13 and 14, respectively). The FT-IR spectra and PXRD of the recovered MOF does not show any significant changes from that of the pristine MOF, suggesting that the structure of the MOF is intact after carboxylation reactions. Inductively coupled plasma atomic emission spectroscopy (ICP-AES) was carried out to determine the leaching of the metal content of CdMOF before and after the carboxylation reaction. There was a very small variation in the metal content of CdMOF before and after CO₂ cycloaddition reactions based on ICP-AES results (28.17% and 28.10% for the activated pristine and recovered CdMOF, respectively). The liquid product (cyclic carbonate) was also analyzed for metal content by ICP-AES, which was found to have traces of Cd ions ~0.35% for the CdMOF sample demonstrating the high chemical and thermal stability of the as-synthesized CdMOF.

**Figure 13.** Infra-red spectra of the as-synthesized and recycled CdMOF after three catalytic cycles.

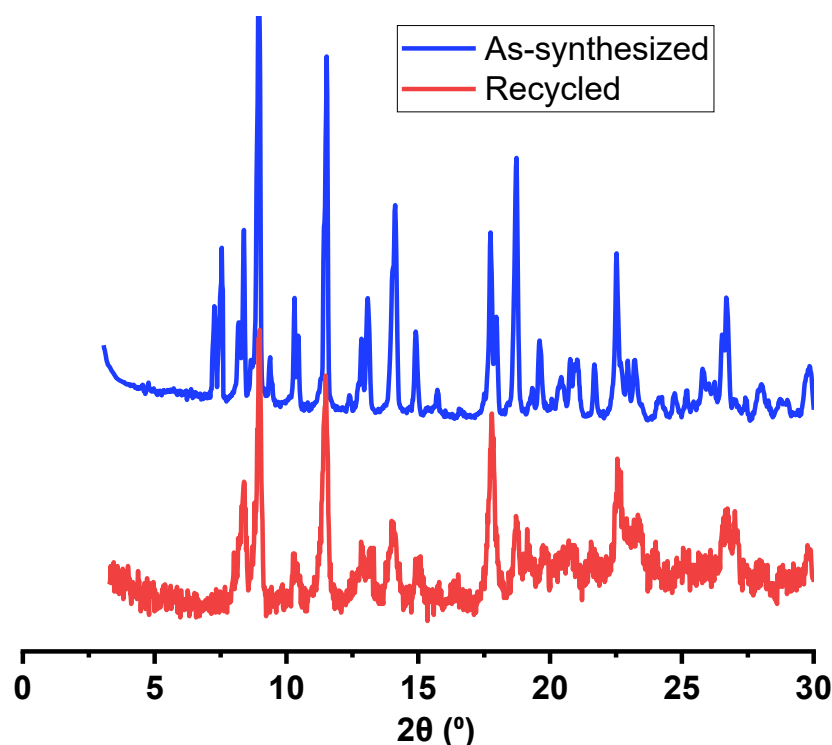


Figure 14. PXRD of the as-synthesized and recycled CdMOF after three catalytic cycles.

The reaction mechanism of the epoxide and CO_2 to give cyclic carbonate has been reported by Miralda et al. [51] and Francis and coworkers [52]. The Lewis acid sites on MOF facilitate the fixation of CO_2 on the substrate (epoxides). It is known that Lewis acid sites on MOFs originate from metal species and Lewis base sites originate from heteroatoms such as nitrogen [51–53]. The CdMOF used in this study has both Lewis acid, Cd(II), and uncoordinated nitrogen atoms, which is expected to favor the binding and activation of the polar “C=O” bond of CO_2 . In working with ZIF-8, Chizallet et al. [53] found that Lewis acid (metal ion) and Lewis base sites, i.e., N-H groups of the coordinated ligand located on the external surface or defected structure can catalyze transesterification reactions. This suggests that the sites located on the external surface or at the defects are more active. Based on the similarities of active sites, that is, Cd(II) species as Lewis acids and uncoordinated –NH groups as Lewis bases, with ZIF-8 [53], which is used as a catalyst for analogous reactions, it can be concluded that the conversion of epoxides to cyclic carbonates using CdMOF is also catalyzed by the active sites on the external surface. Though the catalytic results reported here are preliminary, the catalytic performance of CdMOF compares very well to reported cadmium MOFs. For instance, Parmar and coworkers reported the conversion of ECH into the corresponding cyclic carbonate product in the presence of TBAB as a cocatalyst at 10 bars CO_2 and 80 °C temperature, for 18 h, giving 89% activity [24]. Rachuri and coworkers for ECH in the presence of TBAB, 4 bars of CO_2 , 80 °C temperature, and 8 h, gave 85% activity with >99% selectivity [25]. For ECH in the presence of TBAB, 10 bars CO_2 , 80 °C temperature, and 12 h gave 99% activity [26]. Though these reports use relatively lower temperatures, in all of these reports, CdMOFs are used in combination with co-catalysts (entries 5–7, Table 1). When these MOFs were used without a co-catalyst, the conversion into cyclic carbonates was insignificant (entry 4, Table 1). The literature studies show that a large number of MOFs based on different metal centers are used as a catalyst for the conversion of epoxides to cyclic carbonates. Though better results are reported in some cases but are mostly associated with the use of co-catalyst. [2,54] The efficient MOFs-based catalytic conversions for epichlorohydrin without the use of a cocatalyst are compared. For example, studies by (i) Miralda et al. [51] used ZIF-8 (Zn-MOF) without cocatalyst, the

yield was 44% in 4 h at 7 bar pressure and 80 °C, (ii) Roshan et al. [55], (iii) Macias et al. [56], and (iv) Kuruppathparambil et al. [57] used ZIF-67 (Co-MOF), HKUST-1 (Cu-MOF), and CZ-ZIF (Co-Zn-ZIF) result in 63, 33, and 92% yield, respectively, in 4 h at 7 bar and 100 °C. In all these cases (except CZ-ZIF), though they used mild conditions, the conversion is lower than the CdMOF catalyst used in this work. (v) Ji et al. reported Zr-based MOFs i.e., 66Pym-MeI and 67BPym-MeI, 99 and 87%, respectively, at 100 °C and 5 bars CO₂ pressure in a relatively bit longer period of 24 h [58]. Therefore, the CdMOF may be considered a competent catalyst like MOFs of copper, cobalt, zinc, etc., organic catalysts, and porous organic polymer catalysts [59–62].

4. Conclusions

In summary, we have synthesized a novel CdMOF characterized by FTIR, single crystal, and powder XRD analyses. The thermal stability of the CdMOF was analyzed by TGA and stable up to 200 °C. The Hirshfeld surface analysis was used to explore the supramolecular assembly of the CdMOF. CdMOF efficiently catalyzes epichlorohydrin into cyclic carbonate without using any solvent or co-catalyst. The conversion of epichlorohydrin into cyclic carbonate products was promising. The catalysts were recovered three times without any significant loss in activity or selectivity.

Moreover, the activity of the novel CdMOF was also compared with some of the Cd-based MOFs reported in the literature. The current results revealed that the 3D CdMOF is more active than the previously reported CdMOFs and more interestingly, without using a co-catalyst. It is concluded that the CdMOF could be an appropriate choice for the cyclic addition of CO₂ to epoxides in terms of cost, activity, selectivity, and environmentally friendly.

Supplementary Materials: The following supporting information can be downloaded at: <https://www.mdpi.com/article/10.3390/inorganics10100162/s1>, Figure S1: ¹H-NMR spectra of ligand acid (H₄L); Figure S2: ¹³C-NMR spectra of ligand acid (H₄L); Figure S3: Packing diagram of CdMOF. Selected H-atoms are shown for clarity; Figure S4: ¹H-NMR spectrum in CDCl₃ of the reaction mixture obtained from the conversion of epichlorohydrin after 12 h in absence of catalyst; Figure S5: ¹H-NMR spectrum in CDCl₃ of the reaction mixture obtained from the conversion of epichlorohydrin after 12 h using CdMOF as a catalyst; Table S1: Single crystal XRD experimental description of 3D-CdMOF; Table S2: Selected bond lengths (Å) and angles (°) in CdMOF; Table S3: Hydrogen-bond geometry (Å, °) for CdMOF.

Author Contributions: Conceptualization, F.V., N.A., H.A.Y. and Z.A.K.K.; Methodology, analysis, and investigation, F.V., N.A., H.A.Y., Z.A.K.K., H.U., B.Y., K.S.M., M.A., S.A. and H.M.S.; Writing—original draft & editing, F.V., N.A., H.A.Y., Z.A.K.K., K.S.M. and M.A.; Funding acquisition, resources, and supervision, F.V. All authors have read and agreed to the published version of the manuscript.

Funding: This research received no external funding.

Institutional Review Board Statement: Not applicable.

Informed Consent Statement: Not applicable.

Data Availability Statement: Additional information/data are provided in the supplementary information file.

Acknowledgments: Z.A.K.K., N.A., H.A.Y., H.U., H.M.S. and F.V. gratefully acknowledge “State Key Lab of Advanced Technology for Materials Synthesis and Processing” for financial support.

Conflicts of Interest: The authors declare no conflict of interest.

References

1. Chughtai, A.H.; Ahmad, N.; Younus, H.A.; Laypkov, A.; Verpoort, F. Metal-organic frameworks: Versatile heterogeneous catalysts for efficient catalytic organic transformations. *Chem. Soc. Rev.* **2015**, *44*, 6804–6849. [[CrossRef](#)]
2. Pal, T.K.; De, D.; Bharadwaj, P.K. Metal–organic frameworks for the chemical fixation of CO₂ into cyclic carbonates. *Coord. Chem. Rev.* **2020**, *408*, 213173. [[CrossRef](#)]
3. Al Sharabati, M.; Sabouni, R.; Husseini, G.A. Biomedical applications of metal-organic frameworks for disease diagnosis and drug delivery: A review. *Nanomaterials* **2022**, *12*, 277. [[CrossRef](#)] [[PubMed](#)]

4. Mukhopadhyay, S.; Basu, O.; Nasani, R.; Das, S.K. Evolution of metal organic frameworks as electrocatalysts for water oxidation. *Chem. Commun.* **2020**, *56*, 11735–11748. [[CrossRef](#)] [[PubMed](#)]
5. Ahmad, N.; Younus, H.A.; Gaoke, Z.; Van Hecke, K.; Verpoort, F. Direct synthesis of the 2D copper(II) 5-prop-2-ynoxyisophthalate MOF: Comment on “surface functionalization of porous coordination nanocages via click chemistry and their application in drug delivery”. *Adv. Mater.* **2019**, *31*, 1801399. [[CrossRef](#)] [[PubMed](#)]
6. Batten, S.R.; Hoskins, B.F.; Robson, R. Two interpenetrating 3D networks which generate spacious sealed-off compartments enclosing of the order of 20 solvent molecules in the structures of $Zn(CN)(NO_3)(tpt)_{2/3} \cdot Solv$ ($tpt = 2,4,6$ -tri(4-pyridyl)-1,3,5-triazine, $solv = \sim 3/4 C_2H_2Cl_4 \cdot 3/4 CH_3OH$ or $\sim 3/2 CHCl_3 \cdot 1/3 CH_3OH$). *J. Am. Chem. Soc.* **1995**, *117*, 5385–5386.
7. Ezugwu, C.I.; Mousavi, B.; Asrafa, M.A.; Mehta, A.; Vardhan, H.; Verpoort, F. An n-heterocyclic carbene based MOF catalyst for Sonogashira cross-coupling reaction. *Catal. Sci. Technol.* **2016**, *6*, 2050–2054. [[CrossRef](#)]
8. Ahmad, N.; Chughtai, A.H.; Younus, H.A.; Verpoort, F. Discrete metal-carboxylate self-assembled cages: Design, synthesis and applications. *Coord. Chem. Rev.* **2014**, *280*, 1–27. [[CrossRef](#)]
9. Ezugwu, C.I.; Kabir, N.A.; Yusubov, M.; Verpoort, F. Metal–organic frameworks containing n-heterocyclic carbenes and their precursors. *Coord. Chem. Rev.* **2016**, *307*, 188–210. [[CrossRef](#)]
10. Furukawa, H.; Go, Y.B.; Ko, N.; Park, Y.K.; Uribe-Romo, F.J.; Kim, J.; O’Keeffe, M.; Yaghi, O.M. Isoreticular expansion of metal-organic frameworks with triangular and square building units and the lowest calculated density for porous crystals. *Inorg. Chem.* **2011**, *50*, 9147–9152. [[CrossRef](#)]
11. Farha, O.K.; Eryazici, I.; Jeong, N.C.; Hauser, B.G.; Wilmer, C.E.; Sarjeant, A.A.; Snurr, R.Q.; Nguyen, S.B.T.; Yazaydin, A.Ö.; Hupp, J.T. Metal-organic framework materials with ultrahigh surface areas: Is the sky the limit? *J. Am. Chem. Soc.* **2012**, *134*, 15016–15021. [[CrossRef](#)] [[PubMed](#)]
12. Deng, H.; Yaghi, O.M. Large-pore apertures in a series of metal-organic frameworks. *Science* **2012**, *336*, 1018–1023. [[CrossRef](#)] [[PubMed](#)]
13. Shi, Y.; Yang, A.-F.; Cao, C.-S.; Zhao, B. Applications of MOFs: Recent advances in photocatalytic hydrogen production from water. *Coord. Chem. Rev.* **2019**, *390*, 50–75. [[CrossRef](#)]
14. Qian, Y.; Zhang, F.; Pang, H. A review of mofs and their composites-based photocatalysts: Synthesis and applications. *Adv. Funct. Mater.* **2021**, *31*, 2104231. [[CrossRef](#)]
15. Manna, K.; Zhang, T.; Lin, W. Postsynthetic metalation of bipyridyl-containing metal–organic frameworks for highly efficient catalytic organic transformations. *J. Am. Chem. Soc.* **2014**, *136*, 6566–6569. [[CrossRef](#)] [[PubMed](#)]
16. Forster, P.M.; Cheetham, A.K. Hybrid inorganic–organic solids: An emerging class of nanoporous catalysts. *Top. Catal.* **2003**, *24*, 79–86. [[CrossRef](#)]
17. Farrusseng, D.; Aguado, S.; Pinel, C. Metal–organic frameworks: Opportunities for catalysis. *Angew. Chem. Int. Ed.* **2009**, *48*, 7502–7513. [[CrossRef](#)]
18. Platero Prats, A.E.; de la Peña-O’Shea, V.A.; Iglesias, M.; Snejko, N.; Monge, Á.; Gutiérrez-Puebla, E. Heterogeneous catalysis with alkaline-earth metal-based mofs: A green calcium catalyst. *ChemCatChem* **2010**, *2*, 147–149. [[CrossRef](#)]
19. Liao, T.B.; Ling, Y.; Chen, Z.X.; Zhou, Y.M.; Weng, L.H. A rutile-type porous zinc(II)-phosphonocarboxylate framework: Local proton transfer and size-selected catalysis. *Chem. Commun.* **2010**, *46*, 1100–1102. [[CrossRef](#)]
20. Li, H.; Eddaoudi, M.; O’Keeffe, M.; Yaghi, O.M. Design and synthesis of an exceptionally stable and highly porous metal-organic framework. *Nature* **1999**, *402*, 276. [[CrossRef](#)]
21. Rowsell, J.L.C.; Yaghi, O.M. Metal–organic frameworks: A new class of porous materials. *Microporous Mesoporous Mater.* **2004**, *73*, 3–14. [[CrossRef](#)]
22. Singha, D.K.; Majee, P.; Mondal, S.K.; Mahata, P. A luminescent cadmium based MOF as selective and sensitive iodide sensor in aqueous medium. *J. Photochem. Photobiol. A Chem.* **2018**, *356*, 389–396. [[CrossRef](#)]
23. Xu, X.-D.; Liang, Y.; Mensah, A.; Li, J.-F.; Zhou, L.; Chen, L.-Z.; Wang, F.-M. Synthesis, structures and fluorescence properties of two novel cadmium MOFs based on a tetraphenylethene(TPE)-core ligand. *ChemistrySelect* **2019**, *4*, 12380–12385. [[CrossRef](#)]
24. Parmar, B.; Patel, P.; Kureshy, R.I.; Khan, N.H.; Suresh, E. Sustainable heterogeneous catalysts for CO₂ utilization by using dual ligand Zn(II)/Cd(II) metal-organic frameworks. *Chemistry* **2018**, *24*, 15831–15839. [[CrossRef](#)] [[PubMed](#)]
25. Rachuri, Y.; Kurisingal, J.F.; Chitumalla, R.K.; Vuppala, S.; Gu, Y.; Jang, J.; Choe, Y.; Suresh, E.; Park, D.-W. Adenine-based Zn(II)/Cd(II) metal–organic frameworks as efficient heterogeneous catalysts for facile co₂ fixation into cyclic carbonates: A DFT-supported study of the reaction mechanism. *Inorg. Chem.* **2019**, *58*, 11389–11403. [[CrossRef](#)] [[PubMed](#)]
26. Fan, Y.L.; Li, J.; Ren, Y.; Jiang, H. A ni(salen)-based metal–organic framework: Synthesis, structure, and catalytic performance for CO₂ cycloaddition with epoxides. *Eur. J. Inorg. Chem.* **2017**, *2017*, 4982–4989. [[CrossRef](#)]
27. Zou, Y.; Park, M.; Hong, S.; Lah, M.S. A designed metal-organic framework based on a metal-organic polyhedron. *Chem. Commun.* **2008**, 2340–2342. [[CrossRef](#)]
28. Zou, Y.; Yu, C.; Li, Y.; Lah, M.S. A 3-dimensional coordination polymer with a rare lonsdaleite topology constructed from a tetrahedral ligand. *CrystEngComm* **2012**, *14*, 7174–7177. [[CrossRef](#)]
29. Ahmad, N.; Younus, H.A.; Chughtai, A.H.; Van Hecke, K.; Khattak, Z.A.K.; Gaoke, Z.; Danish, M.; Verpoort, F. Synthesis of 2D MOF having potential for efficient dye adsorption and catalytic applications. *Catal. Sci. Technol.* **2018**, *8*, 4010–4017. [[CrossRef](#)]
30. Wang, G.-Y.; Song, C.; Kong, D.-M.; Ruan, W.-J.; Chang, Z.; Li, Y. Two luminescent metal-organic frameworks for the sensing of nitroaromatic explosives and DNA strands. *J. Mater. Chem. A* **2014**, *2*, 2213–2220. [[CrossRef](#)]

31. Yang, J.-X.; Qin, Y.-Y.; Zhang, X.; Yao, Y.-G. Construction of three new metal-organic frameworks with distinct SBUs: Trinuclear $\{Cd_3(COO)_6\}$ clusters, inorganic -Cd-O-Cd- chains, and heterometallic trinuclear $\{Cd_2ba(COO)_4\}$ clusters. *J. Coord. Chem.* **2016**, *69*, 1568–1576. [[CrossRef](#)]
32. Fu, H.-R.; Wang, F.; Zhang, J. The photoluminescence and gas sorption properties of three Cd(II) mofs based on 1,3,5-benzenetribenzoate with $-NH_2$ or $-OH$ groups. *Dalton Trans.* **2014**, *43*, 4668–4673. [[CrossRef](#)] [[PubMed](#)]
33. Lin, Q.; Wu, T.; Bu, X.; Feng, P. A twelve-connected porous framework built from rare linear cadmium tricarboxylate pentamer. *Dalton Trans.* **2012**, *41*, 3620–3622. [[CrossRef](#)] [[PubMed](#)]
34. Li, N.; Li, Z.-X.; Chen, W.-B.; Yang, M.; Dong, W. Syntheses, structures and photochromic properties of two tetrazolylazo-based K^+ and Cd^{2+} complexes. *J. Coord. Chem.* **2014**, *67*, 3243–3251. [[CrossRef](#)]
35. Zhu, X.-H.; Jiang, D.-Y.; Cheng, X.-C.; Li, D.-H.; Du, W.-G. A Mn(II) complex with an amide-containing ligand: Synthesis, structural characterization, and magnetic properties. *Z. Für Nat. B* **2019**, *74*, 409–414. [[CrossRef](#)]
36. Spackman, P.R.; Turner, M.J.; McKinnon, J.J.; Wolff, S.K.; Grimwood, D.J.; Jayatilaka, D.; Spackman, M.A. Crystalexplorer: A program for hirshfeld surface analysis, visualization and quantitative analysis of molecular crystals. *J. Appl. Crystallogr.* **2021**, *54*, 1006–1011. [[CrossRef](#)]
37. Spackman, M.A.; Jayatilaka, D. Hirshfeld surface analysis. *CrystEngComm* **2009**, *11*, 19–32. [[CrossRef](#)]
38. Ashfaq, M.; Tahir, M.N.; Kuznetsov, A.E.; Mirza, S.H.; Khalid, M.; Ali, A. DFT and single crystal analysis of the pyrimethamine-based novel co-crystal salt: 2,4-diamino-5-(4-chloro-phenyl)-6-ethylpyrimidin-1-ium:4-hydroxybenzoate:Methanol:Hydrate (1:1:1) (DEMH). *J. Mol. Struct.* **2020**, *1199*, 127041. [[CrossRef](#)]
39. Spackman, M.A.; McKinnon, J.J. Fingerprinting intermolecular interactions in molecular crystals. *CrystEngComm* **2002**, *4*, 378–392. [[CrossRef](#)]
40. Ashfaq, M.; Bogdanov, G.; Glebov, V.; Ali, A.; Tahir, M.N.; Abdullah, S. Single crystal investigation, hirshfeld surface analysis and DFT exploration of the pyrimethamine-based novel organic salt: 2, 4-diamino-5-(4-chlorophenyl)-6-ethylpyrimidin-1-ium 3-carboxybenzoate hydrate (1:1:1). *J. Mol. Struct.* **2021**, *1224*, 129309. [[CrossRef](#)]
41. Ashfaq, M.; Ali, A.; Kuznetsov, A.E.; Tahir, M.N.; Khalid, M. DFT and single-crystal investigation of the pyrimethamine-based novel co-crystal salt: 2,4-diamino-5-(4-chlorophenyl)-6-ethylpyrimidin-1-ium-4-methylbenzoate hydrate (1:1:1) (DEMH). *J. Mol. Struct.* **2020**, *1228*, 129445. [[CrossRef](#)]
42. Kargar, H.; Fallah-Mehrjardi, M.; Behjatmanesh-Ardakani, R.; Torabi, V.; Munawar, K.S.; Ashfaq, M.; Tahir, M.N. Sonication-assisted synthesis of new schiff bases derived from 3-ethoxysalicylaldehyde: Crystal structure determination, hirshfeld surface analysis, theoretical calculations and spectroscopic studies. *J. Mol. Struct.* **2021**, *1243*, 130782. [[CrossRef](#)]
43. Kargar, H.; Behjatmanesh-Ardakani, R.; Fallah-Mehrjardi, M.; Torabi, V.; Munawar, K.S.; Ashfaq, M.; Tahir, M.N. Ultrasound-based synthesis, SC-XRD, NMR, DFT, HSA of new Schiff bases derived from 2-aminopyridine: Experimental and theoretical studies. *J. Mol. Struct.* **2021**, *1233*, 130105. [[CrossRef](#)]
44. Ashfaq, M.; Bogdanov, G.; Ali, A.; Tahir, M.N.; Abdullah, S. Pyrimethamine-based novel co-crystal salt: Synthesis, single-crystal investigation, hirshfeld surface analysis and DFT inspection of the 2,4-diamino-5-(4-chlorophenyl)-6-ethylpyrimidin-1-ium 2,4-dichlorobenzoate (1:1) (DECB). *J. Mol. Struct.* **2021**, *1235*, 130215. [[CrossRef](#)]
45. Kargar, H.; Bazrafshan, M.; Fallah-Mehrjardi, M.; Behjatmanesh-Ardakani, R.; Rudbari, H.A.; Munawar, K.S.; Ashfaq, M.; Tahir, M.N. Synthesis, characterization, crystal structures, Hirshfeld surface analysis, DFT computational studies and catalytic activity of novel oxovanadium and dioxomolybdenum complexes with ono tridentate schiff base ligand. *Polyhedron* **2021**, *202*, 115194. [[CrossRef](#)]
46. Kargar, H.; Fallah-Mehrjardi, M.; Behjatmanesh-Ardakani, R.; Munawar, K.S.; Ashfaq, M.; Tahir, M.N. Titanium(IV) complex containing ono-tridentate schiff base ligand: Synthesis, crystal structure determination, hirshfeld surface analysis, spectral characterization, theoretical and computational studies. *J. Mol. Struct.* **2021**, *1241*, 130653. [[CrossRef](#)]
47. Raza, H.; Yildiz, I.; Yasmeeen, F.; Munawar, K.S.; Ashfaq, M.; Abbas, M.; Ahmed, M.; Younus, H.A.; Zhang, S.; Ahmad, N. Synthesis of a 2D copper(II)-carboxylate framework having ultrafast adsorption of organic dyes. *J. Colloid Interface Sci.* **2021**, *602*, 43–54. [[CrossRef](#)]
48. Turner, M.J.; McKinnon, J.J.; Jayatilaka, D.; Spackman, M.A. Visualisation and characterisation of voids in crystalline materials. *CrystEngComm* **2011**, *13*, 1804–1813. [[CrossRef](#)]
49. Ali, A.; Khalid, M.; Tahir, M.N.; Imran, M.; Ashfaq, M.; Hussain, R.; Assiri, M.A.; Khan, I. Synthesis of diaminopyrimidine sulfonate derivatives and exploration of their structural and quantum chemical insights via SC-XRD and the DFT approach. *ACS Omega* **2021**, *6*, 7047–7057. [[CrossRef](#)]
50. Amor, S.B.; Jacquet, M.; Fioux, P.; Nardin, M. XPS characterisation of plasma treated and zinc oxide coated pet. *Appl. Surf. Sci.* **2009**, *255*, 5052–5061. [[CrossRef](#)]
51. Miralda, C.M.; Macias, E.E.; Zhu, M.; Ratnasamy, P.; Carreon, M.A. Zeolitic imidazole framework-8 catalysts in the conversion of CO_2 to chloropropene carbonate. *ACS Catal.* **2012**, *2*, 180–183. [[CrossRef](#)]
52. Mousavi, B.; Chaemchuen, S.; Moosavi, B.; Luo, Z.; Gholampour, N.; Verpoort, F. Zeolitic imidazole framework-67 as an efficient heterogeneous catalyst for the conversion of CO_2 to cyclic carbonates. *New J. Chem.* **2016**, *40*, 5170–5176. [[CrossRef](#)]
53. Chizallet, C.; Lazare, S.; Bazer-Bachi, D.; Bonnier, F.; Lecocq, V.; Soyer, E.; Quoineaud, A.-A.; Bats, N. Catalysis of transesterification by a nonfunctionalized metal-organic framework: Acido-basicity at the external surface of ZIF-8 probed by FTIR and ab initio calculations. *J. Am. Chem. Soc.* **2010**, *132*, 12365–12377. [[CrossRef](#)] [[PubMed](#)]

54. Liang, J.; Huang, Y.-B.; Cao, R. Metal–organic frameworks and porous organic polymers for sustainable fixation of carbon dioxide into cyclic carbonates. *Coord. Chem. Rev.* **2019**, *378*, 32–65. [[CrossRef](#)]
55. Kuruppathparambil, R.R.; Jose, T.; Babu, R.; Hwang, G.-Y.; Kathalikkattil, A.C.; Kim, D.-W.; Park, D.-W. A room temperature synthesizable and environmental friendly heterogeneous ZIF-67 catalyst for the solvent less and co-catalyst free synthesis of cyclic carbonates. *Appl. Catal. B Environ.* **2016**, *182*, 562–569. [[CrossRef](#)]
56. Macias, E.E.; Ratnasamy, P.; Carreon, M.A. Catalytic activity of metal organic framework $\text{Cu}_3(\text{BTC})_2$ in the cycloaddition of CO_2 to epichlorohydrin reaction. *Catal. Today* **2012**, *198*, 215–218. [[CrossRef](#)]
57. Kuruppathparambil, R.R.; Babu, R.; Jeong, H.M.; Hwang, G.-Y.; Jeong, G.S.; Kim, M.-I.; Kim, D.-W.; Park, D.-W. A solid solution zeolitic imidazolate framework as a room temperature efficient catalyst for the chemical fixation of CO_2 . *Green Chem.* **2016**, *18*, 6349–6356. [[CrossRef](#)]
58. Ji, H.; Naveen, K.; Lee, W.; Kim, T.S.; Kim, D.; Cho, D.-H. Pyridinium-functionalized ionic metal–organic frameworks designed as bifunctional catalysts for CO_2 fixation into cyclic carbonates. *ACS Appl. Mater. Interfaces* **2020**, *12*, 24868–24876. [[CrossRef](#)]
59. Wan, Y.-L.; Wang, L.; Wen, L. Amide-functionalized organic cationic polymers toward enhanced catalytic performance for conversion of CO_2 into cyclic carbonates. *J. CO_2 Util.* **2022**, *64*, 102174. [[CrossRef](#)]
60. Hao, Y.; Yan, X.; Chang, T.; Liu, X.; Kang, L.; Zhu, Z.; Panchal, B.; Qin, S. Hydroxyl-anchored covalent organic crown-based polymers for CO_2 fixation into cyclic carbonates under mild conditions. *Sustain. Energy Fuels* **2022**, *6*, 121–127. [[CrossRef](#)]
61. Yang, Y.; Guo, Y.; Yuan, J.; Xie, H.; Gao, C.; Zhao, T.; Zheng, Q. Agile construction of porous organic frameworks pending carboxylic acids and imidazolium-based ionic liquids for the efficient fixation of CO_2 to cyclic carbonates. *ACS Sustain. Chem. Eng.* **2022**, *10*, 7990–8001. [[CrossRef](#)]
62. Yuan, G.; Lei, Y.; Meng, X.; Ge, B.; Ye, Y.; Song, X.; Liang, Z. Metal-assisted synthesis of salen-based porous organic polymer for highly efficient fixation of CO_2 into cyclic carbonates. *Inorg. Chem. Front.* **2022**, *9*, 1208–1216. [[CrossRef](#)]